SCA2003-07: CORRELATION OF DYNAMIC IMMISCIBLE DISPLACEMENT PATTERNS WITH THE FRACTIONAL WETTABILITY OF POROUS MEDIA

V. Sygouni[1,2], C. D. Tsakiroglou[1,*], A. C. Payatakes[1,2]
[1]FORTH / ICE-HT, Stadiou Street, Platani, P.O. Box 1414, GR – 26504 Patras, Greece
[2]Department of Chemical Engineering, University of Patras, GR – 26504 Patras, Greece

This paper was prepared for presentation at the International Symposium of the Society of Core Analysts held in Pau, France, 21-24 September 2003

ABSTRACT

Effects of the fractional pore surface wettability on the dynamic two-phase immiscible displacement patterns in porous media are examined experimentally. A model porous medium of controlled fractional wettability is fabricated by mixing neutral-wet glass microspheres with oil-wet PTFE microspheres, and packing them between two transparent glass plates. Visualization experiments of the displacement of the oleic by the aqueous phase are performed on the model porous medium at a low value of the capillary number by varying the number fraction of oil-wet particles. The displacement growth pattern is compact in areas of uniform wettability and is dominated by capillary fingering in areas where the heterogeneity of wettability is quite large. The transient response of the pressure drop across the porous medium is correlated with the spatial distribution of the critical capillary pressures required for the menisci advancement in individual throats and chambers and clusters of interconnected throats and chambers of varying wettability. The amplitude and frequency of the observed pressure drop fluctuations are associated with successive isons and rheons occurring during the motion of menisci between positions of capillary stability and instability. Such information can be used as a "fingerprint" of the spatial variation of the pore surface fractional wettability.

INTRODUCTION

The wettability of a rock surface with respect to a fluid system is of key importance for a variety of multiphase flow processes occurring in reservoir rocks, as for instance the displacement of crude oil by water [6,12,16,21,22]. Wettability expresses the affinity of a surface for water or oil and is governed by the interaction of short range surface forces [11] which, in turn, depend on rock mineralogy, pH and salinity of brine, and crude oil composition [3,9,11,13]. Because of the spatial variation of the aforementioned factors over the porous formation, very often the wettability of a rock surface may be heterogeneous (fractional, mixed), in which case distinct regions of the rock surface exhibit different affinity for oil or water [4]. The wettability of rocks is commonly quantified by the Amott, Amott-Harvey and USBM macroscopic indices [4,17]. However, these indices are complex functions of pore size distribution, pore space connectivity and wettability

* Corresponding author, e-mail: ctsakir@iceht.forth.gr, Tel.: 2610 965212, Fax: 2610 965223

[7,8], and hence they don't provide explicit information about the spatial distribution and relative percentages of oil-wet and water-wet pore surface in a fractional-wet porous medium. Advanced techniques, such as the analysis of NMR relaxation times, can give only qualitative information concerning the establishment of mixed wettability conditions in a porous medium, where crude oil ageing changes the larger pores from water-wet to oil-wet while the smaller pores remain unaltered [10]. Visualization experiments performed in Hele-Shaw cells suggest that the displacement front could be used to quantify the effect of wettability on the displacement process and thus on the fluid recovery [5]. On the other hand, it is well-known that the transient response of the pressure drop across a pore network is a "fingerprint" of the dominated flow pattern [1,2] whereas successive fluctuations of the capillary pressure are associated with the variability of pore sizes and may be employed to obtain information concerning the pore space geometry from rate-controlled porosimetry data [19,23]. In the present work, immiscible displacement visualization experiments are performed at very low values of the capillary number in a two-layer model porous medium consisting of pores of identical size and variable but controlled fractional wettability. The spatial variation of wettability is correlated with the transient displacement pattern, and the pressure drop measured across the porous medium. The ultimate objective of the work is to suggest a procedure for analyzing the results of unsteady displacement experiments performed on cores, in order to extract quantitative information concerning the distribution of fractional wettability on the pore-wall surfaces of a porous medium.

METHODS AND MATERIALS

The model porous medium consists of glass and PTFE micro-spheres of identical diameter (=0.15 cm) packed between two cover glass plates (Fig.1a) with a silicon rubber gasket. Five holes drilled at the two ends of the upper plate serve as inlet and outlet ports, whereas four other holes drilled in its central area are used for the filling of the model with spherical particles. The fluids used in displacement experiments were silicon oil and deionized water colored with methylene blue (Table 1). The interfacial tension was measured in a tensiometer (KRUSS K-8) by using the ring method, whereas the equilibrium contact angle q_e was measured on glass and PTFE plates under a stereoscope (Nikon SMZ1000) by using the sessile drop method and image analysis. The fractional wettability of the porous medium was adjusted by mixing neutral-wet glass spheres with strongly oil-wet PTFE spheres at varying number fractions of the oil-wet particles, f_p, ranging from 0 to 1. In a typical experiment, the pore space is filled completely with oil (defender), which is then displaced by water (invader) injected at constant influx rate through a syringe pump (HARVARD PHD 2000) (Fig.1b). With the aid of a high precision differential pressure transducer (VALIDYNE DP45) operating over a low pressure range (0-850 Pa), the pressure drop across the porous medium is measured every 2-20 s and transmitted to a data acquisition card installed in the host computer. At equal time intervals snap-shots of the displacement are captured with a CCD camera (AW-E300 Panasonic), transmitted to an image grabber (DIGITSUITE MATROX) and recorded on the hard disk of the PC (Fig.1b).

The absolute permeability of the porous medium was measured and found $k = 1500\,D$ (apparent cross-section area = model width X micro-sphere diameter). All experiments were done at a very low value of the capillary number ($Ca = \mu_o u / ?_{ow}$): Ca=1.26 x 10^{-8} so that the viscous pressure drop across the entire porous medium was two orders of magnitude smaller than the average capillary pressure required for throat invasion. In this manner, the assumption of quasi-static displacement is reasonable, and transient fluctuations of the capillary pressure, arising from pore space morphology and spatial variation of wettability, are reflected directly in the measured pressure drop signal. The Bond number is smaller than unity and any gravity effects on the fluid distribution between the two layers may be ignored.

PORE NETWORK PROPERTIES

The porous medium can be regarded as a two-layer (3-dimensional) throat-and-chamber network composed of two interconnected triangular lattices (Fig.2a). In each layer throats T1 are formed between two spherical particles and one cover plate (Fig.2b), pore chambers are formed among any three particles touching each other and one of the cover plates, whereas the narrowest cross-sectional area of chambers (Fig.2c) coincides with the vertical throats T2 interconnecting the two layers. The number fractions of the two types of throats in the network are: f_{T1}=0.75 and f_{T2}=0.25. The percolation probability, p, is defined as the fraction of throats that can be crossed by the invading phase, and is given by the relation:

$$p = \int_0^{J_{ti}} h_t(J)\,dJ \tag{1}$$

where $h_t(J)$ is a critical curvature distribution function of throats, and its upper limit J_{ti} is determined by the equilibrium capillary pressure, P_{ct}, according to the relation:

$$P_{ct} = g_{ow} J_{ti} \tag{2}$$

The bond percolation threshold of a regular lattice can be approximated as:

$$p_{cb} = \frac{d}{z(d-1)} \tag{3}$$

where d is the dimensionality and z is the coordination number [18]. Consequently, it is $p_{cb,3} = 0.375$ (z=4, d=3) and $p_{cb,2} = 0.66$ (z=3, d=2) for the 3-D (two-layer) and 2-D (one-layer) lattices, respectively.

Fractional wettability

The fractional wettability of the porous medium is defined by the fraction of oil-wet particles, f_p. It is worth noting that the pore surface is fractional-wet not only at the network scale but also at the scale of individual throats and chambers. Depending on the wetting state of the surrounding solid surface, various classes of throats and chambers can be distinguished (Table 2).

The number fraction of each class of pores was calculated from the probability of its appearance in the network (Table 2). The critical capillary pressure required for the invasion of aqueous phase in a throat was estimated by using the approximate force balance:

$$P_{ct} = \frac{(L_1 \cos q_1 + L_2 \cos q_2) g_{ow}}{A} \quad (4)$$

where A is the throat cross-sectional area, and L_1, L_2 are the lengths of the throat perimeter with contact angles $?_1$ and $?_2$, respectively (Table 2). Because of the irregular shape of chambers, instead of a point value an "average" value of the equilibrium capillary pressure encountered within a pore chamber was estimated by using the approximate relation:

$$P_{cc} = \frac{(A_1 \cos q_1 + A_2 \cos q_2) g_{ow}}{V} \quad (5)$$

where V is the chamber volume and A_1, A_2 are the areas of the chamber surface with contact angles $?_1$ and $?_2$ respectively (Table 2). Two factors have been overlooked in Eqs.(4) and (5): (i) pendular rings of displaced fluid may remain in the contact regions of solid particles, and the minimum capillary pressure required for a meniscus invasion in a throat may be smaller than that given by Eq.(4) [15]; (ii) for finite values of the contact angle, the capillary pressure encountered in a pore of converging / diverging geometry may take its maximum value downstream the throat rather than at its narrowest cross-section area [20]. The equations of Table 2 enable us to estimate the critical curvature distribution functions of throats, $h_t(J)$ and chambers, $h_c(J)$ and interpret qualitatively the experimental results.

RESULTS AND DISCUSSION

The displacement used in the experiments is a drainage process in which the wetting oleic phase (o) is being displaced by the neutrally-wetting aqueous phase (w). It is well known that low values of the viscosity ratio $? = \mu_w / \mu_o$ favor viscous fingering at high Ca values and capillary fingering at low Ca values [14]. As the wettability changes gradually from neutral-wet (f_p=0) to oil-wet (f_p=1) the spatial distribution of the critical curvatures of throats and chambers changes (Table 2). Specifically, as f_p increases the mean curvatures J_{mt} and J_{mc} increase, while the width of $h_t(J)$ and $h_c(J)$ initially increase, until they reach some maximum values, and then decrease. In areas of almost uniform wettability, the critical curvature distributions of throats and chambers are narrow, the simultaneous menisci advancement in neighboring throats and chambers is favored, and compact flow patterns arise (Figs.3a and 6a). In areas of heterogeneous wettability the spatial variation of the critical capillary pressures, required for throat and chamber invasion increases, menisci advancement in the various classes of throats and chambers takes place over a broad range of capillary pressures, and the creation of capillary fingers is favored (Figs.3a, 4a, 5a). Because of the small magnitude of the viscous forces compared to the capillary ones, the pressure drop measured across the pore network is equivalent to an "instantaneous" capillary pressure averaged over the interfacial configurations of the entire network. In flow rate controlled experiments, the observed fluctuations of the pressure drop across the

pore network (Figs.3b-6b) are associated with successive “isons” and “rheons” explained in detail below.

Continuous chains of oil-wet throats act as capillary barriers to advancing menisci, and the imposed pressure difference across the pore network must be increased to exceed the local capillary resistance so that the aqueous phase/oil phase menisci penetrate into a region of high curvature (ison). When the imposed pressure difference across the network exceeds the local critical capillary pressure for throat invasion, the invading phase may proceed from a region of high curvature to a region of low curvature. Then, a sudden drop of the pressure difference occurs, so that the local fluid saturation is redistributed and the total saturation remains almost unaltered (rheon). Successive isons and rheons may take place without any spatial variation on wettability as menisci move from stable (throat) to unstable (chamber) positions [23] (Fig.3b). As f_p increases, the spatial heterogeneity of wettability intensifies, and the frequency and amplitude of pressure drop fluctuations increase (Fig.3b-5b). At sufficiently high f_p values the spatial variation of fractional wettability in the pore network weakens so that the pressure drop fluctuations are damped out (Fig.6b), and the maximum value of the measured pressure drop (Fig.6b) gives an estimate of the breakthrough pressure (Fig.6a). The approximate relationships shown in Table 2 were used to estimate rough discrete values of the critical curvature distribution of throats $h_t(J)$ (Fig.7a-d). The critical curvature for invasion in throats T2 is commonly higher than that for invasion in throats T1 (Fig.7a-d), so that the advance of displacement across one of the layers may be preferred against its simultaneous spreading in both layers, particularly with reference to intermediate f_p values (Figs.4,5). For intermediate f_p values the percolation probability of the two first classes of throats T1 (Figs.7b, 7c) is comparable to or exceeds the percolation threshold of the 2-D network, $p_{cb,2}$, so that a network spanning cluster of the aqueous phase is created at a relatively low capillary pressure, and a substantial amount of oil phase is bypassed and remains in the pore network after breakthrough (Figs.4a, 5a). For high f_p values the breakthrough pressure is relatively high (Fig.7d), and extensive displacement occurs in both layers (Fig.6a), either through the menisci advancement in T2 throats or through the simultaneous growth of two displacement fronts (Fig.6a).

High frequency and small amplitude fluctuations of the measured pressure drop across the network arise from successive isons/rheons caused by the existence of positions of capillary stability and instability in the pore network, because of differences between the sizes of throats and chambers [19,23]. Such events may shadow isons/rheons caused by the spatial variation of wettability. In order to eliminate pore structure noise from the experimental results, the measured pressure drop was smoothed out by using Fast Fourier Transform (FTT), rejecting several (10-30) high frequency components of the transformed data, and using Inverse FFT to rebuild $DP(t)$ (Fig.7e-7h). The shape of $DP(t)$ up to the time where breakthrough of the aqueous phase takes place (Fig.7e-7h) is consistent with the critical curvature distribution of throats (Fig.7a-7d). The more heterogeneous the wettability, the wider the distribution $h_t(J)$ (Fig.7a-c) and the wider the distribution of the

amplitude of $DP(t)$ fluctuations (Fig.7e-g). The smaller the variability of the (fractional) wettability (Fig.7d), the narrower the distribution $h_t(J)$, and the narrower the observed distribution of the $DP(t)$ amplitude (Fig.7h).

CONCLUSIONS

Visualization experiments performed at low Ca values on chamber-and-throat networks of identical pore sizes and varying fractional wettability indicated that the displacement growth pattern is correlated with the spatial variation of wettability. Specifically, a compact displacement growth pattern is observed in areas characterized by a small variability of wettability, whereas capillary fingering dominates over areas where the spatial variation of wettability is quite large. The transient response of the pressure drop across the porous medium is related explicitly with the spatial distribution of the critical capillary pressures of menisci motion in individual throats and chambers as well as in clusters of interconnected pores of varying wettability. The amplitude and frequency of the observed pressure drop fluctuations is associated with successive isons and rheons, and such information may be used as a "fingerprint" of the spatial variation of the pore surface fractional wettability.

REFERENCES

1. Aker, E., and Maloy, K.J., "Simulating temporal evolution of pressure in two-phase flow in porous media", *Phys Rev. E* (1998) **58**, 2217-2226.
2. Aker, E, Maloy, K.J., Hansen, A., and Batrouni, G.G., "A two-dimensional network simulator for two-phase flow in porous media", *Transp. Porous Media* (1998) **32**, 163-186.
3. Anderson, W.G., "Wettability literature survey-Part 1: rock/oil/brine interactions and the effects of core handling on wettability", *J. Pet. Technol.* (1986) **Oct.**, 1125-1144.
4. Anderson, W.G., "Wettability literature survey-Part 2: wettability measurement", *J. Pet. Technol.* (1986) **Nov.**, 1246-1262.
5. Araujo, Y.C., and Araujo, M., "Geometrical description of contact angle line fluctuations in heterogeneous systems with controlled wettability", *J. Colloid Interface Sci.* (2000) **229**, 92-101.
6. Cuiec, L.E., "Evaluation of reservoir wettability and its effects on oil reservoir", *Interfacial Phenomena in Oil Recovery*, N.R. Morrow (ed.), Marcel Dekker, New York (1990), 319-375.
7. Dixit, A.B., Buckley, J.S., McDougall, S.R., and Sorbie, K.S., "Empirical measures of wettability in porous media and the relationships between them derived from pore-scale modeling", *Transp. Porous Media* (2000) **40**, 27-54.
8. Dominguez, A., Perez-Aguilar, H., Rojas, F., and Kornhauser, I., "Mixed wettability : a numerical study of the consequences of porous media morphology", *Colloids and Surfaces A: Phys. & Eng. Aspects* (2001) **187-188**, 415-424.
9. Drummond, C., and Israelachvili, J., "Surface forces and wettability", *J. Pet. Sci. Eng.* (2002) **33**, 123-133.

10. Guan, H., Brougham, D., Sorbie, K.S., and Packer, K.J., "Wettability effects in a sandstone reservoir and outcrop cores from NMR relaxation time distributions", *J. Pet. Sci. and Eng.* (2002) **34**, 35-54.
11. Hirasaki, G.J., "Wettability: fundamentals and surface forces", *SPEFE* (1991) **June**, 217-226.
12. Jadhunandan, P.P. and Morrow, N.R., "Effect of wettability on waterflood recovery for crude-oil/brine/rock systems", *SPERE* (1995) **Feb.**, 40-46.
13. Kovscek, A.R., Wong, H. and Radke, C.J., "A pore-level scenario for the development of mixed wettability in oil reservoirs", *AIChE J.* (1993) **39**, 1072-1085.
14. Lenormand, R., Touboul, E., and Zarcone, C., "Numerical models and experiments on immiscible displacement in porous media", *J. Fluid Mech.* (1988) **189**, 165-187.
15. Mayer, R.P. and Stowe, R.A., "Mercury porosimetry-breakthrough pressure for penetration between packed spheres", *J. Colloid Sci.* (1965) **20**, 893-911.
16. Schramm, L.L., and Mannhardt, K., "The effect of wettability on foam sensitivity to crude oil in porous media", *J. Pet. Sci. and Eng.* (1996) **15**, 101-113.
17. Sharma, M.M. and Wunderlich, R.W., "The alteration of rock properties due to interaction with drilling fluid components", *J. Pet. Sci. Eng.* (1987) **1**, 127-143.
18. Stauffer, D. and Aharony, A., Introduction to Percolation Theory, Taylor & Francis, London (1992).
19. Toledo, P.G., Scriven, L.E., and Davis, H.T., "Pore-space statistics and capillary pressure curves from volume controlled porosimtery", *SPEFE* (1994) **March**, 46-54.
20. Tsakiroglou, C.D. and Payatakes, A.C.,"A new simulator of mercury porosimetry for the characterization of porous materials", *J. Colloid Interface Sci.* (1990) **137**, 315-339.
21. Tsakiroglou, C.D. and Fleury, M., "Resistivity index of fractional wettability porous media", *J. Pet. Sci. Eng.* (1999) **22**, 253-274.
22. Tzimas, G.C., Matsuura, T., Avraam, D.G., van der Brugghen, W., Constantinides, G.N., and Payatakes, A.C., "The combined effect of the viscos ity ratio and the wettability during forced imbibition through nonplanar porous media", *J. Colloid Interface Sci.* (1997) **189**, 27-36.
23. Yuan, H.H., and Swanson, B.F., "Resolving pore-space characteristics by rate-controlled porosimetry", *SPEFE* (1989) **March**, 17-24.

Table 1. Physicochemical properties of fluid system

Silicon oil density, $?_?$ (kg/m^3)	970
Silicon oil viscosity, μ_o (Pa s)	0.033
Deionized water density, $?_w$ (kg/m^3)	995
Deionized water viscosity, μ_w (Pa s)	0.001
Interfacial tension, $?_{ow}$ (N/m)	32 10^{-3}
*Silicon oil/water/glass contact angle, $?_1$ (^{o})	90
*Silicon oil/water/PTFE contact angle, $?_2$ (^{o})	0

* Measured from the side of oleic phase

Table 2. Classification of throats and chambers with respect to fractional wettability

Throat type	*Wetting state of surrounding particles	**Normalized probability	Dimensionless curvature radius, JR
T1	nw-nw	$(1-f_p)^2 f_{T1}/f_N$	$(4+2p)\cos q_1/(4-p)$
T1	nw-ow	$f_p(1-f_p)f_{T1}/f_N$	$[(4+2p)\cos q_1 + p\cos q_2]/(4-p)$
T1	ow-ow	$f_p{}^2 f_{T1}/f_N$	$[4\cos q_1 + 2p\cos q_2]/(4-p)$
T2	nw-nw-nw	$(1-f_p)^3 f_{T2}/f_N$	$p\cos q_1/(\sqrt{3}-p/2)$
T2	nw-nw-ow	$f_p(1-f_p)^2 f_{T2}/f_N$	$(2p\cos q_1 + p\cos q_2)/[3(\sqrt{3}-p/2)]$
T2	nw-ow-ow	$f_p{}^2(1-f_p)f_{T2}/f_N$	$(p\cos q_1 + 2p\cos q_2)/[3(\sqrt{3}-p/2)]$
T2	ow-ow-ow	$f_p{}^3 f_{T2}/f_N$	$p\cos q_2/(\sqrt{3}-p/2)$
Chamber type	***Wetting state of surrounding particles**	****Normalized probability**	**Dimensionless curvature radius, JR**
C1	nw-nw-nw	$(1-f_p)^3/f_N$	$\dfrac{(p+\sqrt{3})\cos q_1}{(\sqrt{3}-p/3)}$
C1	nw-nw-ow	$f_p(1-f_p)^2/f_N$	$\dfrac{(2p/3+\sqrt{3})\cos q_1 + p\cos q_2/3}{(\sqrt{3}-p/3)}$
C1	nw-ow-ow	$f_p{}^2(1-f_p)/f_N$	$\dfrac{(p/3+\sqrt{3})\cos q_1 + 2p\cos q_2/3}{(\sqrt{3}-p/3)}$
C1	ow-ow-ow	$f_p{}^3/f_N$	$\dfrac{\sqrt{3}\cos q_1 + p\cos q_2}{(\sqrt{3}-p/3)}$

* nw=neutral-wet (contact angle=$?_1$), ow=oil-wet (contact angle=$?_2$)

** Normalization factor: $f_N = f_{T1}(1+f_p{}^2 - f_p) + f_{T2}(1+2f_p{}^2 - 2f_p)$

*** Normalization factor: $f_N = 1+2f_p{}^2 - 2f_p$

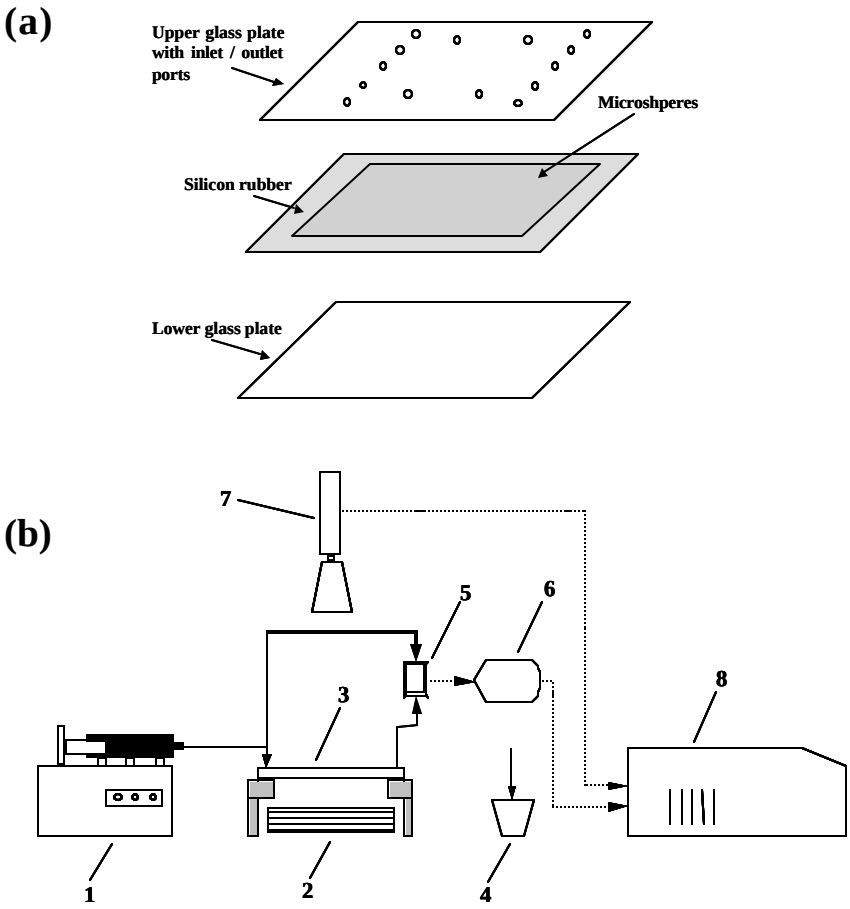

Figure 1. (a) Components of the model porous medium. (b) Schematic diagram of the experimental apparatus: 1=syringe pump, 2=light source, 3=model porous medium, 4=waste storage tank, 5=differential pressure transducer, 6=pressure display, 7=video-camera with zoom-lens, 8=host computer equipped with image capturing and data acquisition cards.

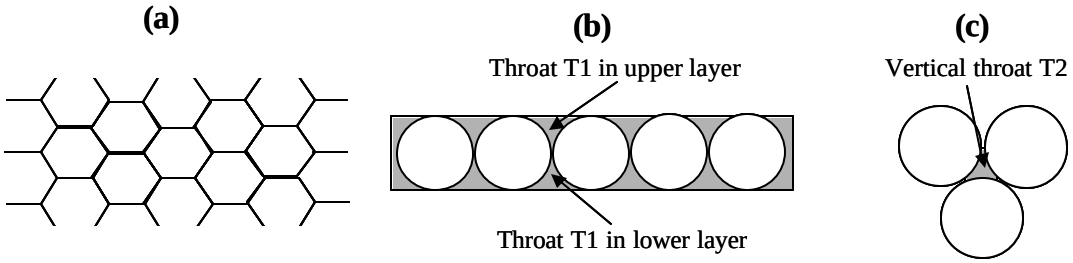

Figure 2. (a) Topology of bond (throat)-and-node(chamber) network in each layer. (b) Throats of type T1. (c) Vertical throats of type T2.

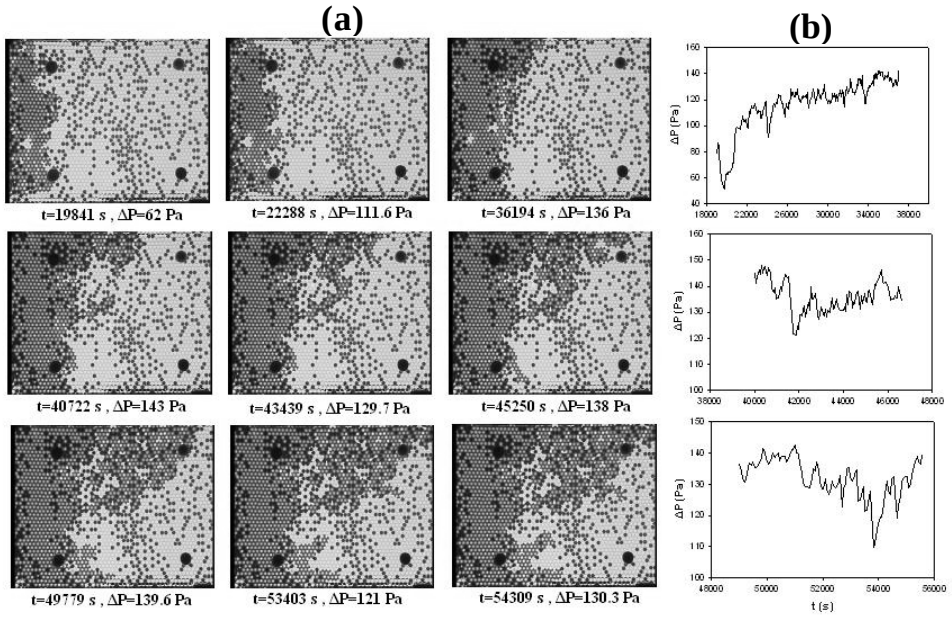

Figure 3. (a) Snap-shots of the immiscible displacement of silicon oil (white) by aqueous phase (blue) in a model porous medium with f_p=0.25. The glass particles are transparent, whereas the PTFE particles are opaque and appear black. (b) Transient response of the pressure drop across the porous medium (Ca=1.26 x 10^{-8}).

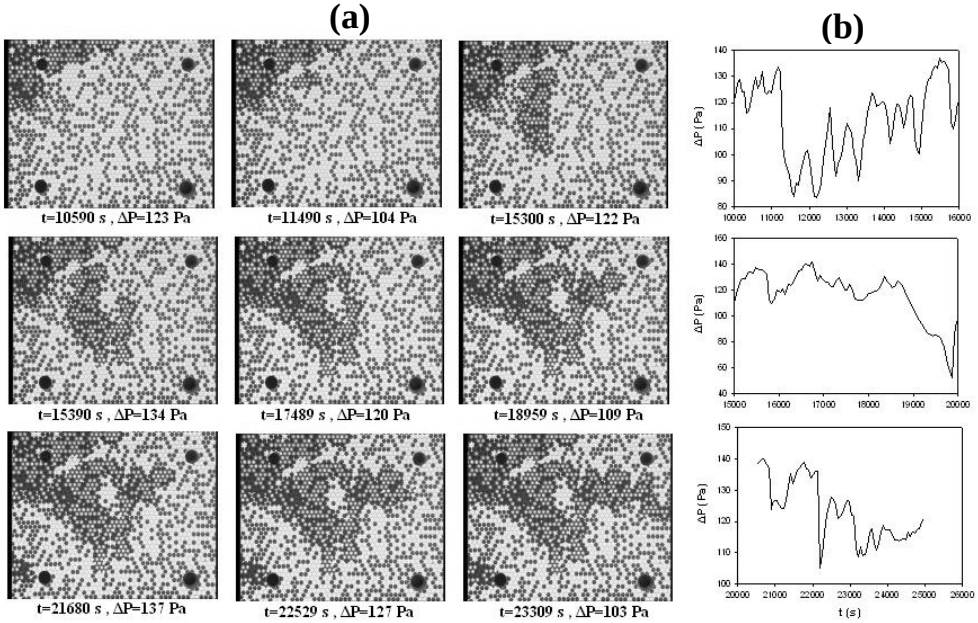

Figure 4. (a) Snap-shots of the immiscible displacement of silicon oil (white) by aqueous phase (blue) in a model porous medium with f_p=0.44. The glass particles are transparent, whereas the PTFE particles are opaque and appear black. (b) Transient response of the pressure drop across the porous medium (Ca=1.26 x 10^{-8}).

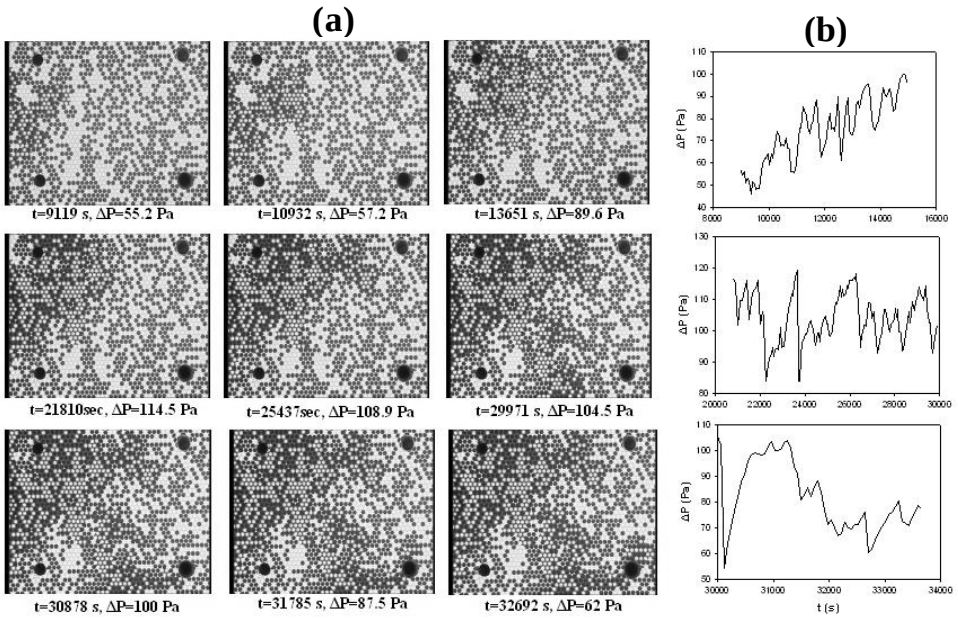

Figure 5. (a) Snap-shots of the immiscible displacement of silicon oil (white) by aqueous phase (blue) in a model porous medium with f_p=0.57. The glass particles are transparent, whereas the PTFE particles are opaque and appear black. (b) Transient response of the pressure drop across the porous medium (Ca=1.26 x 10^{-8}).

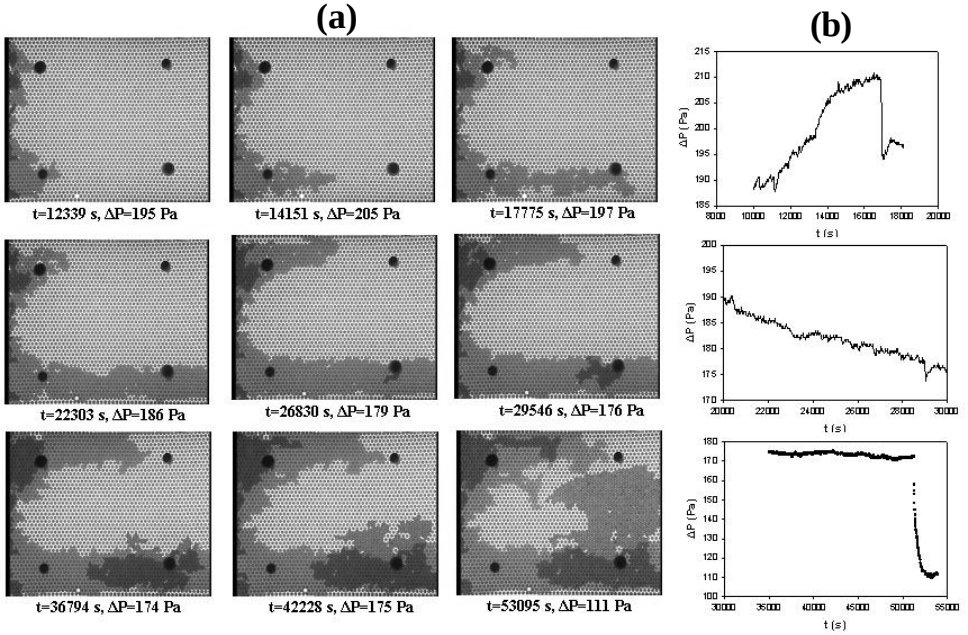

Figure 6. (a) Snap-shots of the immiscible displacement of silicon oil (white) by aqueous phase (blue) in a model porous medium with f_p=1.0. The glass particles are transpa rent, whereas the PTFE particles are opaque and appear black. (b) Transient response of the pressure drop across the porous medium (Ca=1.26 x 10^{-8}).

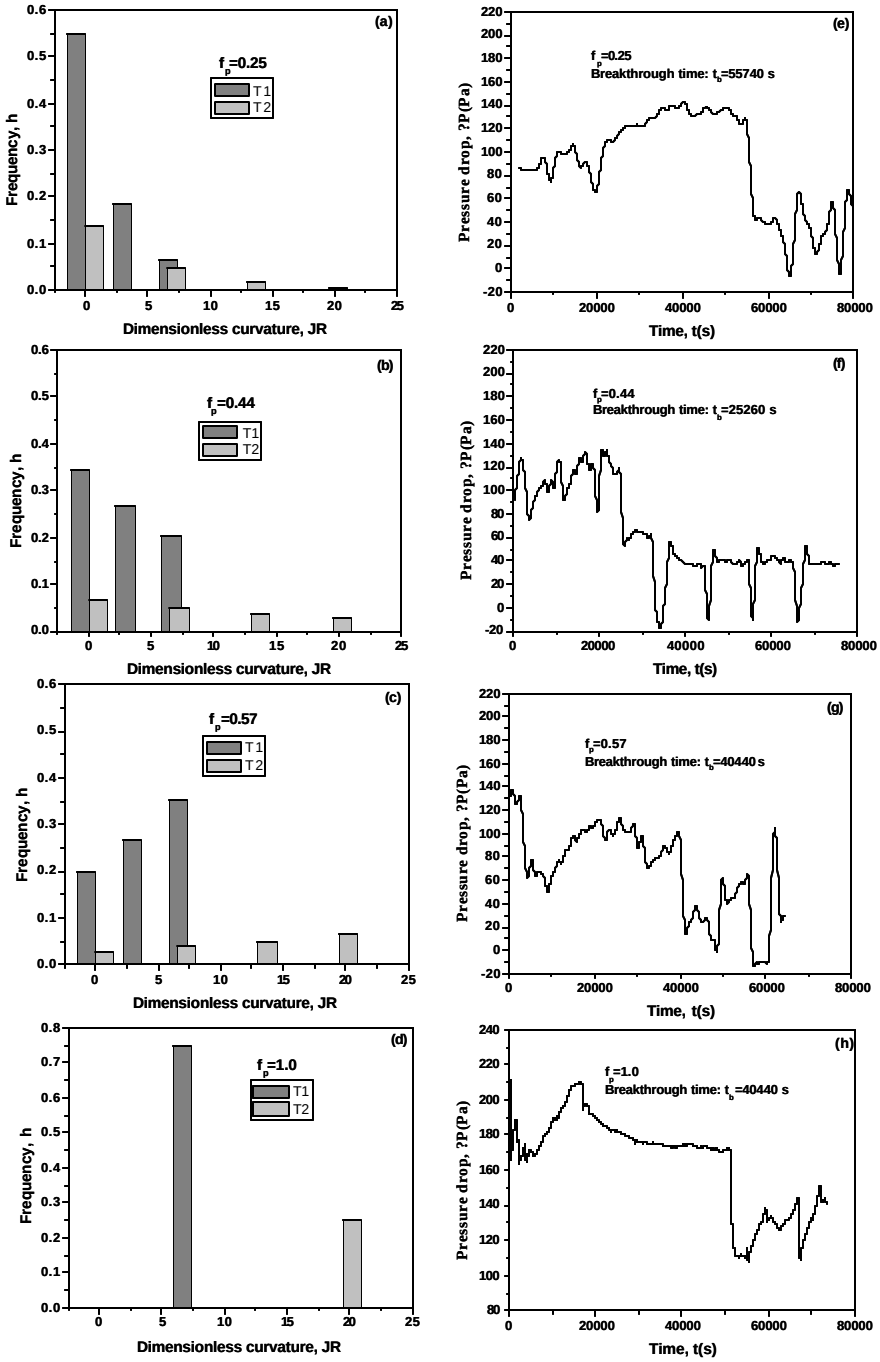

Figure 7. (a-d) Critical curvature frequency distribution of throats for various values of f_p. (e-h) Smoothed transient response of the pressure drop across the porous medium for various values of f_p (Ca=1.26 x 10^{-8}).